SCIENTIFIC REPORTS

OPEN

First principles calculation of the nonhydrostatic effects on structure and Raman frequency of 3C-SiC

Liu Lei[1,2], Yi Li[1], Liu Hong[1], Li Ying[1,2], Zhuang Chun-Qiang[3], Yang Long-Xing[1] & Liu Gui-Ping[1]

For understanding the quantitative effect of nonhydrostatic stress on properties of material, the crystal structure and Raman spectra of 3C-SiC under hydrostatic and nonhydrostatic stress were calculated using a first-principles method. The results show that the lattice constants (*a*, *b*, and *c*) under nonhydrostatic stresses deviate those under hydrostatic stress. The differences of the lattice constants under hydrostatic stress from nonhydrostatic stresses with differential stress were fitted by linear equation. Nonhydrostatic stress has no effect on density of 3C-SiC at high pressure, namely the equations of state of 3C-SiC under hydrostatic stress are same as those under nonhydrostatic stress. The frequencies and pressure dependences of LO and TO modes of 3C-SiC Raman spectra under nonhydrostatic stress are just same as those under hydrostatic stress. Under nonhydrostatic stress, there are four new lines with 361, 620, 740, and 803 cm^{-1} appeared in the Raman spectra except for the LO and TO lines because of the reduction of structure symmetry. However the frequencies and pressure dependences of the four Raman modes remain unchanged under different nonhydrostatic stresses. Appearance of new Raman modes under nonhydrostatic stress and the linear relationship of the differences of lattice constants under hydrostatic and nonhydrostatic stresses with differential stress can be used to indicate state of stress in high pressure experiments. The effect of nonhydrostatic stress on materials under high pressure is complicated and our calculation would help to understanding state of stress at high pressure experiments.

Diamond anvil cells (DACs) have long been extensively used to generate high pressure on materials for research purposes. Recently, extreme pressures to 750 GPa has been achieved using DACs with improved design[1]. However, maintaining hydrostatic conditions under such extreme pressures has long been a great challenge. Generally at low pressures, hydrostatic conditions in DACs can be well maintained by proper experimental set-ups, such as gaskets thickness, sample size, sample chamber diameter, and choice of pressure-transmitting media (PTM). But at extreme high pressure, pressure induced solidification of the PTM is inevitable and effects of non-hydrostatic stress caused by PTM solidification will become more and more ineligible with increasing pressure. The stress in the PTM and the sample will both begin to depart from hydrostatic under extreme pressures.

Nonhydrostatic stress has been reported to have unique influence on material. Powder diffraction lines tend to broaden significantly under nonhydrostatic stresses[2,3]. The phase transformations of a number of compounds show strong dependence of transformation pressure and sequence on nonhydrostatic stress[4–12]. The pressure dependencies of crystal parameters of aegirine ($NaFeSi_2O_6$) measured by the diffraction experiments showed anomalies at 12.62 GPa and above under nonhydrostatic stress[13]. The decrease of magnetic moment of bcc iron with increasing pressure under nonhydrostatic stress is faster than those under hydrostatic stress[14]. The density, lattice strain and elastic constants of forsterite under differential stress are different from those of under hydrostatic stress and the difference increase with increasing differential stress[15]. The Raman modes shifting their frequencies to either higher or lower values, relative to its equivalent value under hydrostatic pressure, depend on the state of differential stress[16].

Studies of the state of nonhydrostatic stress in high pressure experiment have thus received considerable attentions. Two distinct theories have been proposed with the anisotropic elasticity theory (AET)[17–22] and the isotropic elasticity theory (IET)[23–28]. These theories were used to analyze the state of nonhydrostatic stress in high pressure

[1]Key Laboratory of Earthquake Prediction, Institute of Earthquake forecasting, China Earthquake Administration, Beijing, 100036, China. [2]National Key Laboratory of Shock Wave and Detonation Physics, Mianyang, 621900, China. [3]Institute of Microstructure and Properties of Advanced Materials, Beijing University of Technology, Beijing, 100124, China. Correspondence and requests for materials should be addressed to L.L. (email: liulei@cea-ies.ac.cn)
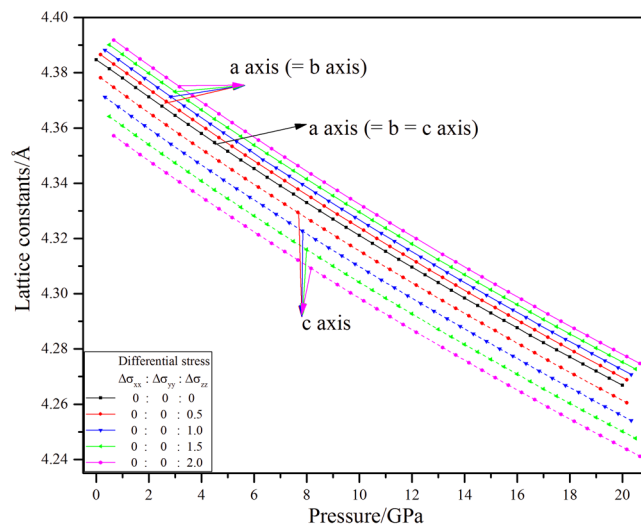
Figure 1. Lattice constants of 3C-SiC under different stresses.

experiments by deriving relationship of lattice strain, d-spacing, and the diffraction data. Estimation of nonhydrostatic stress using IET and AET requires the knowledge of the crystal structure parameters and elastic moduli of the material under hydrostatic stress. Due to the difference of the lattice strain and elastic constant of materials under non-hydrostatic and hydrostatic stress[15,16], quantitatively studies of lattice parameters under nonhydrostatic stress are essential understanding the state of nonhydrostatic stress under high pressure. However, quantitatively investigation is both time consuming and difficult to practice due to the poor repeatability of high-pressure experiments. First-principles methods made great success in calculating material properties[29–37] including the state of nonhydrostatic (differential) stress and its effects at atomic scale[15,16,38–45]. Therefor it is suitable used for this works.

The cubic 3C-SiC with the zinc blende crystal possesses the nearest to the diamond structure in both carbon and silicon. The 3C-SiC possesses high chemical stability and high bulk and shear modulus, 220 GPa and 183 GPa, respectively[46–50]. The 3C-SiC crystal transforms to a rocksalt phase at 66GPa[46]–100GPa[51] and maintains stable till 2373 K[52]. Meanwhile, as a cubic crystal, it is easy to clarify the relationship between lattice strain and nonhydrostatic stress. So 3C-SiC is an ideal sample for studying the effect of differential stresses on materials properties. Here we report our first-principle calculation about the effect of nonhydroustatic stress on crystal structure and Raman spectrum of 3C-SiC.

Results and Discussion

Lattice parameters. Figure 1 shows lattice constants of 3C-SiC as a function of stress. Additional pressures were put following *z* direction (*c*-axis) for producing the nonhydrostatic stresses during pressuring. As a cubic symmetrical crystal, the lattice constants a, b, and c are equal and all three bond angles (α, β, and γ) are 90°. However under nonhydrostatic stresses, the lattice constants of 3C-SiC are not equal (a = b ≠ c), so the 3C-SiC cannot keep cubic symmetry under nonhydrostatic stress. The lattice constants under nonhydrostatic stresses deviate those under hydrostatic stress. The *a* and *b* (*a* = *b*) are larger than their equivalent hydrostatic values under nonhydrostatic stresses; however, those of *c* are smaller. Namely, the effect of nonhydrostatic stresses on the lattice constants shows the Poisson effect that consistent with previous results[15,16].

The differences of lattice constants of 3C-SiC between nonhydrostatic and hydrostatic stresses were presented in Fig. 2. Obviously, effect of nonhydrostatic stress on lattice constants linearly increases with increasing differential stress. The difference of the lattice constants (*a*, *b*, and *c*) under hydrostatic stress from nonhydrostatic stresses with differential stress were fitted by a linear equation as follows:

$$\text{For } \boldsymbol{a} \text{ and } \boldsymbol{b}, \quad \mathbf{D} = 0.0054\mathbf{S_D} - 1\text{E-5}, \quad R^2 = 1 \tag{1}$$

$$\text{For } \boldsymbol{c}, \quad \mathbf{D} = 0.012\mathbf{S_D} - 2\text{E-4}, \quad R^2 = 1 \tag{2}$$

where **D** (unit, Å) indicates the differences in lattice constants under hydrostatic and nonhydrostatic stresses; $\mathbf{S_D}$ (unit, GPa) indicates the amount of differentials stress.

The effect of nonhydrostatic stress on *c* axis is about 2.2 times that of *a* and *b* axis because *a* and *b* axis simultaneously increase, however only *c* axis decrease under nonhydrostatic stresses. Those linear relations are help to understand state of nonhydrostatic stress in high pressure experiments.

Density/Equation of State. The densities of 3C-SiC under hydrostatic and nonhydrostatic stresses are shown in Fig. 3. It is very hard to find some differences among the densities under hydrostatic and nonhydrostatic stresses. Even from the partial enlarged figure, the densities under different stress also are identical. They
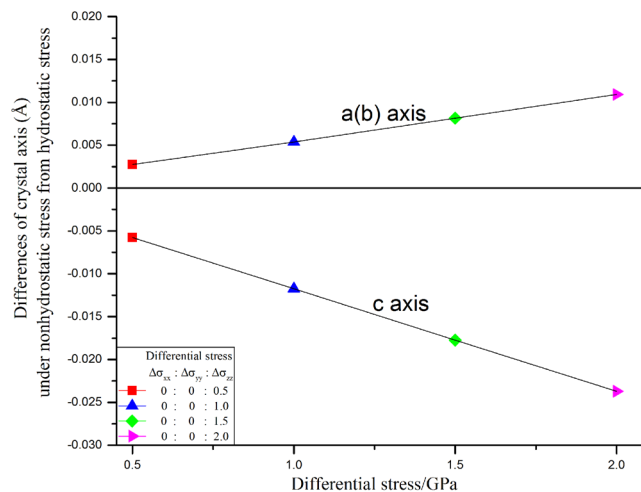
Figure 2. The differences of lattice constants under hydrostatic and nonhydrostatic stresses.
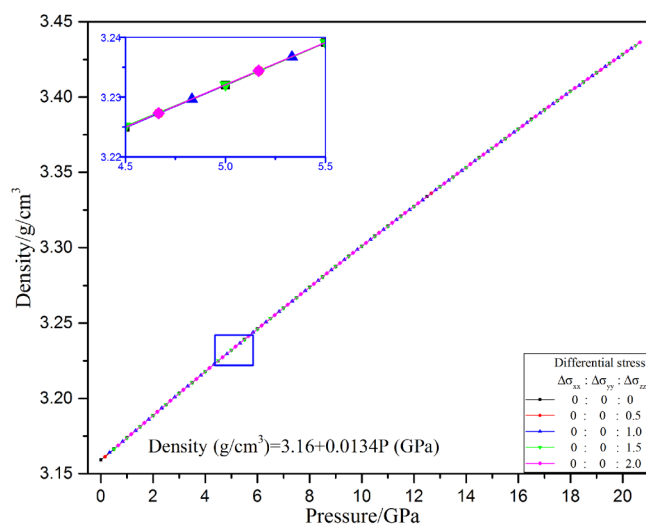

Figure 3. Variation of density of 3C-SiC with different stress conditions.

all linearly increase with increasing pressure. The linear equation was used to describe the relationship of density and pressure as

$$Density \ (g/cm^3) = 3.16 + 0.0134P \ (GPa) \tag{3}$$

The result indicates that nonhydrostatic stress has no effect on cell volume of 3C-SiC at high pressure, namely the equations of state of 3C-SiC under hydrostatic stress are same as those under nonhydrostatic stress. The result is different with the effect of nonhydrostatic stress on density of forsterite[15] and calcite[16]. The density of calcite and forsterite increases or decreases under different differential stress, relative to its equivalent values under hydrostatic pressure, depend on the state of differential stress. So the effect of nonhydrostatic stress on density of materials under high pressure is complicated. More works need to be done on effect of nonhydrostatic stress on equation of state of materials.

Raman modes. Raman scattering conveys structural information about the lattice vibrational properties of solids. Because of difference in the electronegativity of Si and C, the optical modes of 3C-SiC at Γ point of Brillouin zone are split into two degenerate transverse optical modes (TO) and a nondegenerate longitudinal optical mode (LO)[53]. The pressure derivative of the LO and TO modes and LO-TO splitting that got in this work and previous researches under hydrostatic stress are listed in Table 1. The Raman frequencies of 3C-SiC were obtained by experiment[53–55] with 795.9–797.7 cm^{-1} (TO) and 972.9–973.6 cm^{-1} (LO) and by calculation[55,56] with 783–784 cm^{-1} (TO) and 956–958 cm^{-1} (LO). Our calculated TO and LO modes agree with the previous experimental and calculated data and the differences are within 3%. The TO and LO lines shift to higher frequencies with increasing

	ν_0	dν/dP	ν_0	dν/dP	ν_0	dν/dP	ν_0	dν/dP
TO	797.7	3.88	797.2	3.46	774.1	3.65	783.7	3.813
LO	973.6	4.59	973.8	4.27	942.3	4.25	958.5	4.417
LO-TO	175.9	0.654	176.6	0.812	168.6	0.578	174.8	0.604
Method	Expt.				Calc.			
References	[55]		[53]		This works		[55]	

Table 1. Pressure dependence of Raman frequencies of 3C-SiC under hydrostatic stress. Phonon frequencies ν_0 are in cm^{-1} and dν/dP in cm^{-1}/GPa. Note: The results refer to fits of linear functions for experimental data.
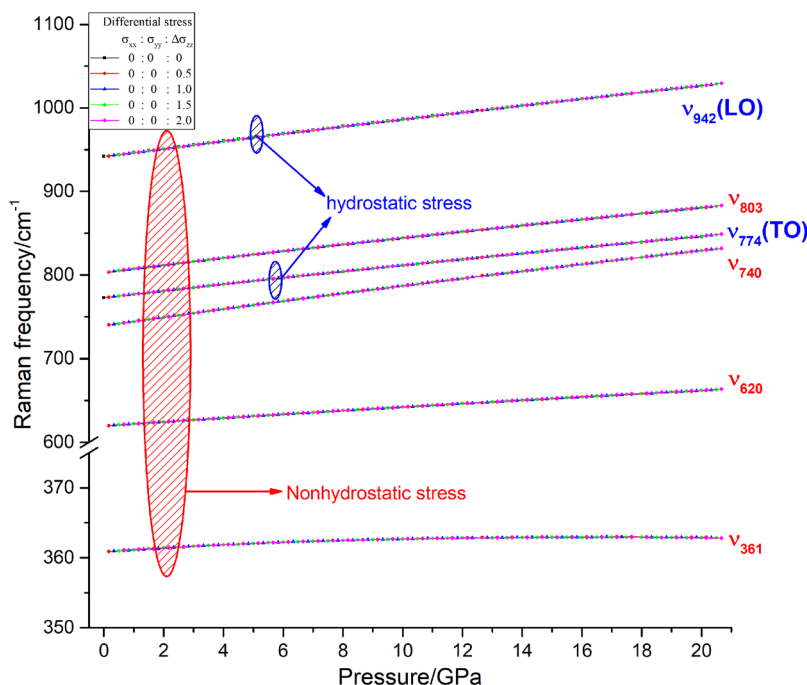

Figure 4. Variation of Raman frequencies of 3C-SiC with pressure.

pressure. The LO-TO splitting also increase with increasing pressure because of an unusually increase of the ionicity of 3C-SiC under pressure that caused by charge transfer from Si to C[57].

The pressure dependences of the Raman frequencies of 3C-SiC under hydrostatic and nonhydrostatic stress are displayed in Fig. 4. Under hydrostatic stress, only two Raman frequencies of 3C-SiC show in the Raman spectrum, namely LO and TO lines. However under nonhydrostatic stress, there are four new lines with 361, 620, 740, and 803 cm^{-1} appeared in the Raman spectra except for the LO and TO lines because of the reduction of crystal structure symmetry. The pressure dependences of LO and TO modes under nonhydrostatic stress are just same as those under hydrostatic stress. For the 4 new Raman modes (361, 620, 740, and 803 cm^{-1}), their frequencies linear increase with increasing pressure and their pressure derivative are 0.1, 2.1, 4.6, and 3.9 cm^{-1}/GPa.

However the frequencies and pressure dependences of the 4 Raman modes remain unchanged under these 4 different nonhydrostatic stress states. Namely for all Raman modes of 3C-SiC, the states of nonhydrostatic stress have no effect on frequency and pressure dependence. However the activity of 4 new Raman frequencies decrease with increasing pressure and mean the effect of nonhydrostatic the Raman spectrum weaken under high pressure (Fig. 5). Though nonhydrostatic stresses have no effect on Raman frequency and its pressure derivative of 3C-SiC, the new appeared Raman modes under nonhydrostatic stress can be used to indicate state of stress in the high experiment. Therefor those results can help to understanding state of stress at high pressure experiments. Because the differential stresses have no effect pressure dependence of the Raman frequencies, we only list the phonon dispersion of 3C-SiC under hydrostatic stress with 0, 10, and 20 GPa as Fig. 6. The phonon dispersion relation spectrum show consistent results with pressure dependences of the Raman frequencies.

Computational Method

Computational background.
First principles calculations were performed by density functional perturbation theory (DFPT)[58], density functional theory (DFT)[59,60] and plane wave pseudopotential technique, as implemented in CASTEP-2017 codes[61]. The generalized gradient approximation (GGA-PBE) was used to describe exchange-correlation interactions[62]. Norm Conserving Pseudopotential[63] was employed to model electron-ion interaction. A $8 \times 8 \times 8$ Monkhorst Pack grid of k points was adopted for sampling Brillouin zone. A convergence criterion of 5×10^{-7} a.u. on the total energy was used in the self-consistent field (SCF) calculations. The energy
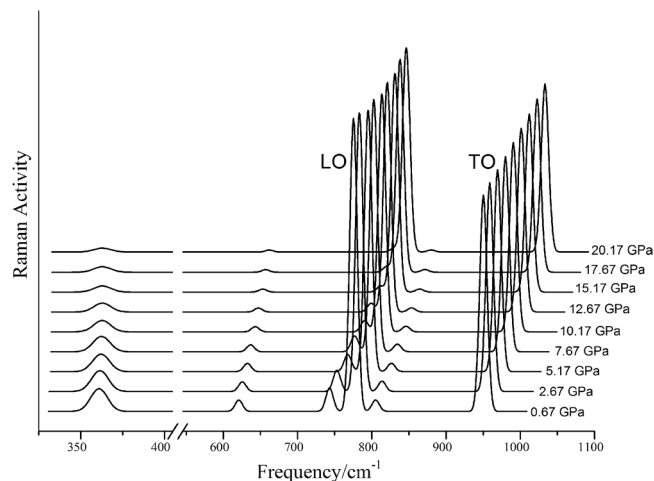
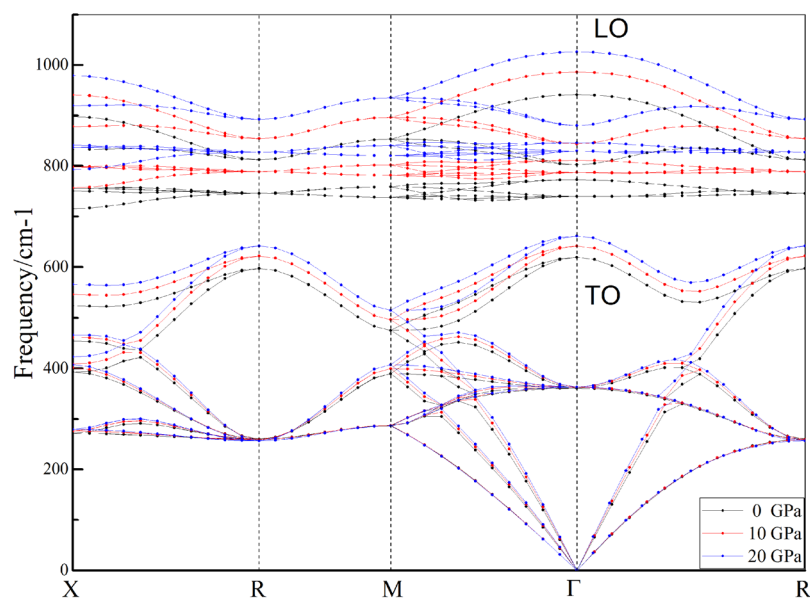**Figure 5.** Raman spectrum of 3C-SiC under nonhydrostatic stress.

Figure 6. Phonon dispersions of 3C-SiC along the main symmetry directions.

cutoff for plane wave basis was chosen as 900 eV. Geometrically-optimized convergence criterion used in energy, maximum force, maximum stress, and maximum displacement are 5×10^{-6} eV/atom, 0.01 eV/Å, 0.02 GPa, and 5×10^{-4} Å, respectively.

The structure and Raman spectroscopy of 3C-SiC at given pressures were calculated by optimizing simultaneously both lattice constants and atomic positions based on the consideration that Hellmann–Feynman forces and stresses applied respectively on nuclei and lattice parameters were minimized, respectively[64]. Spatial derivatives of the macroscopic polarization were calculated numerically along eigenvectors of each Raman active phonon mode according to the polarization for each displacement using linear response formalism[65]. Once these derivatives are determined, the Raman cross-section through appropriate averaging space can be calculated. Further details can be found in Porezag and Pederson[66] and Refson *et al.*[58].

Different stresses were applied to the crystal along *a*, *b*, and *c* axis directions (i.e., x, y, and z direction). They were marked as σ_{xx}, σ_{yy}, and σ_{zz}, which were schematically illustrated in Fig. 7. Thus, the equivalent hydrostatic pressure (*P*, GPa) applied to crystals is $(\sigma_{xx} + \sigma_{yy} + \sigma_{zz})/3$. When $\sigma_{xx} = \sigma_{yy} = \sigma_{zz}$, the pressure is hydrostatic; when $\sigma_{xx} \neq \sigma_{yy}$ or σ_{zz}, the pressure is nonhydrostatic. Therefore, if σ_{xx} is equal to P_1, σ_{yy} is equal to P_1, and σ_{zz} is equal to $P_1 + x$ GPa, then P is equal to *(3P₁+x)/3* GPa, differential stress is $\sigma_{xx} = \sigma_{xx} - P = -x/3$ GPa, $\sigma_{yy} = \sigma_{yy} - P = -x/3$ GPa, and $\sigma_{zz} = \sigma_{zz} - P = 2x/3$ GPa. The largest stress difference among σ_{zz}, σ_{yy}, and σ_{xx} is *x* GPa. Here, effects of five sets of different stresses including hydrostatic pressure (namely, x = 0, 0.5, 1, 1.5 and 2 GPa) on the structure and Raman spectrum of 3C-SiC were calculated.

Lattice constant (Å)			
a	Method	Reference	
4.361	Calc.	[46]	
4.365	Calc.	[48]	
4.360	Expt.	[50]	
4.326	Expt.	[47]	
4.348	Calc.	This works	
Elastic modulus (GPa)			
Bulk modulus (GPa)	Shear modulus (GPa)		
196.2		Calc.	[67]
212		Calc.	[46]
200		Calc.	[48]
211		Calc.	[49]
225.2		Calc.	[68]
224		Expt.	[50]
248		Expt.	[69]
211.4	183.5	Expt.	[70]
208.7	186.4	Calc.	This works
Raman frequency			
TO	LO		
795.9	972.9	Expt.	[54]
797.7	973.6	Calc.	[55]
783	956	Calc.	[56]
772.7	941.1	Calc.	This works

Table 2. Structural, elastic, and Raman characters of 3C-SiC under ambient condition.
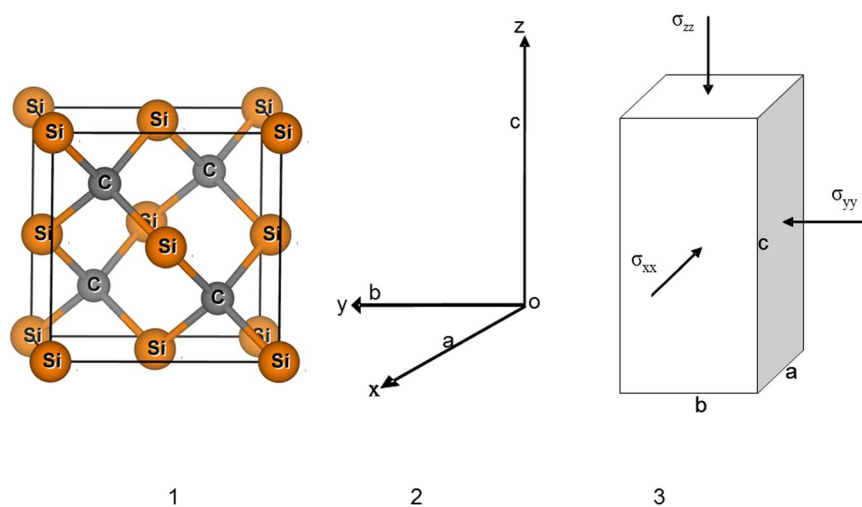

Figure 7. Atomic structure of 3C-SiC and schematic diagram of differential stress project. (1) Atomic structure of 3C-SiC, (2) Lattice constants and directions, and (3) Applied stresses (σ_{xx}, σ_{yy}, and σ_{zz}).

Benchmark calculation. To assess the performance of the DFT and DFPT total-energy approach used here, we performed test calculations on the structural and elastic of 3C-SiC (Table 2). The close agreement between previous results and our calculations demonstrates the validity of our computational method. The results indicate that the calculation approach well replicates the properties of 3C-SiC.

References

1. Dubrovinsky, L. *et al.* The most incompressible metal osmium at static pressures above 750 gigapascals. *Nature* **525**(7568), 226–229 (2015).
2. Weidner, D. J., Wang, Y. & Vaughan, M. T. Yield strength at high pressure and temperature. *Geophys. Res. Lett.* **21**, 753 (1994).
3. Singh, A. K., Liermann, H. P. & Saxena, S. K. Strength of magnesium oxide under high pressure: evidence for the grain-size dependence. *Solid State Commun.* **132**, 795 (2004).

4. Jayaraman, A. *et al*. Pressure-induced phase transitions in $CuGeO_3$ from Raman spectroscopic studies. *J. Raman Spectrosc.* **32**, 167 (2001).
5. Badro, J. *et al*. Theoretical study of a five-coordinated silica polymorph. *Phys. Rev. B* **56**, 5797 (1997).
6. Ma, Y. Z., Selvi, E. & Levitas, I. V. Effect of shear strain on the $\alpha-\varepsilon$ phase transition of iron: a new approach in the rotational diamond anvil cell. *J. Phys: Condens. Matter.* **18**, S1075 (2006).
7. Caspersen, K. J., Lew, A. & Ortiz, M. Importance of Shear in the bcc-to-hcp Transformation in Iron. *Phys. Rev. Lett.* **93**, 115501 (2004).
8. Ji, C. *et al*. Shear-induced phase transition of nanocrystalline hexagonal boron nitride to wurtzitic structure at room temperature and lower pressure. *PNAS* **109**(47), 19111 (2012).
9. Levitas, V. I. High-density amorphous phase of silicon carbide obtained under large plastic shear and high pressure. *Phys. Rev. B* **85**(5), 054114 (2012).
10. Levitas, V. I. & Zarechnyy, O. M. Modeling and simulation of strain-induced phase transformations under compression and torsion in a rotational diamond anvil cell. *Phys. Rev. B* **82**(17), 174124 (2010).
11. Taniguchi, T. *et al*. Effect of nonhydrostaticity on the pressure induced phase transformation of rhombohedral boron nitride. *Appl. Phys. Lett.* **70**(18), 2392–2394 (1997).
12. Levitas, V. I., Hashemi, J. & Ma, Y. Z. Strain-induced disorder and phase transformation in hexagonal boron nitride under quasi-homogeneous pressure: *In situ* X-ray study in a rotational diamond anvil cell. *Europhys Lett.* **68**(4), 550–556 (2004).
13. Downs, R. T. & Singh, A. K. Analysis of deviatoric stress from nonhydrostatic pressure on a single crystal in a diamond anvil cell: The case of monoclinic aegirine, $NaFeSi_2O_6$. *J. Phys. Chem. Solids* **67**, 1995 (2006).
14. Lu, Z. *et al*. Structure phase transition from α to ε in Fe under non-hydrostatic pressure: an ab initio study. *Acta. Physica Sinica* **58**(3), 2083–2089 (2009).
15. Liu, L. *et al*. Effect of differential stress on the structure and Raman spectra of calcite from first-principles calculations. *Am. Mineral.* **101**(8), 1892–1897 (2016).
16. Liu, L. *et al*. Differential stress effect on structural and elastic properties of forsterite by first principles simulation. *Phys. Earth Planet. Inter.* **233**, 95–102 (2014).
17. Singh, K. *et al*. Recent Trends in High Pressure Research, Oxford & IBH, New Delhi, (1992).
18. Uchida, T., Funamori, N. & Yagi, T. Lattice strains in crystals under uniaxial stress field. *J. Appl. Phys.* **80**, 739 (1996).
19. Funamori, N., Yagi, T. & Uchida, T. Deviatoric stress measurement under uniaxial compression by a powder x-ray diffraction method. *J. Appl. Phys.* **75**, 4327 (1994).
20. Duffy, T. S. *et al*. Equation of state and shear strength at mulitmegabar pressure: magnesium oxide to 227 GPa. *Phys. Rev. Lett.* **74**, 1371 (1995).
21. Hemley, R. J. *et al*. X-ray imaging of stress and strain of diamond, iron, and tungsten at megabar pressures. *Science* **276**, 1242 (1996).
22. Duffy, T. S. *et al*. Elasticity, shear strength, and equation of state of molybdenum and gold from x-ray diffraction under nonhydrostatic compression to 24 GPa. *J. Appl. Phys.* **86**, 6729 (1999).
23. Ruoff, A. L. Yield stress determination as a function of pressures at very high pressures. *Scripta Metall.* **8**, 1161 (1974).
24. Kinsland, G. L. & Bassett, W. A. Modification of the diamond cell for measuring strain and the strength of materials at pressures up to 300 kilobar. *Rev. Sci. Instrum.* **47**, 130 (1976).
25. Kinsland, G. L. & Bassett, W. A. Strength of MgO and NaCl polycrystals to confining pressures of 250 kbar at 25 °C. *J. Appl. Phys.* **48**, 978 (1977).
26. Mao, H. K. *et al*. Specific volume measurements of Cu, Mo, Pd, and Ag and calibration of the ruby R1 fluorescence pressure gauge from 0.06 to 1 Mbar. *J. Appl. Phys .* **49**, 3276 (1978).
27. Ruoff, A. L. *et al*. Miniaturization techniques for obtaining static pressures comparable to the pressure at the center of the earth: X-ray diffraction at 416 GPa. *Rev. Sci. Instrum.* **61**, 3830 (1990).
28. Jeanloz, R., Godwal, B. K. & Meade, C. Static strength and equation of state of rhenium at ultra-high pressures. *Nature* **349**, 687 (1991).
29. Jahn, S. & Kowalski, P. Theoretical approaches to structure and spectroscopy of earth materials. *Rev. Miner. Geochem.* **78** (2014).
30. Gillan, M. J. *et al*. First-principles modeling of Earth and planetary materials at high pressures and temperatures. *Rep. Prog. Phys.* **69**, 2365–2441 (2006).
31. Wentzcovitch, R. & Stixrude, L. Theoretical and computational methods in mineral physics: geophysical applications. *Rev. Miner. Geochem.* **71** (2010).
32. Wang, J., Ma, F., Liang, W., Wang, R. & Sun, M. Optical, photonic and optoelectronic properties of graphene, h-NB and their hybrid materials. *Nanophotonics* **6**(5), 943 (2017).
33. Wang, J., Cao, S., Ding, Y., Ma, F., Lu, W. & Sun, M. Theoretical investigations of optical origins of fluorescent graphene quantum dots. *Sci. Rep.* **6**, 24850 (2016).
34. Wang, J., Ma, F. & Sun, M. Graphene, hexagonal boron nitride, and their heterostructures: properties and applications. *RSC Adv.* **7**, 16801 (2017).
35. Mu, X. *et al*. Analysis and design of resonance Raman reporter molecules by density functional theory. *J. Raman Spectrosc.* **48.9**, 1196 (2017).
36. Wang, J., Xu, X., Mu, X., Ma, F. & Sun, M. Magnetics and spintronics on two-dimensional composite materials of graphene/hexagonal boron nitride. *Materials Today Physics* **3**, 93 (2017).
37. Wang, J., Ma, F., Liang, W. & Sun, M. Electrical properties and applications of graphene, hexagonal boron nitride (h-BN), and graphene/h-BN heterostructures. *Materials Today Physics* **2**, 6 (2017).
38. Parrinello, M. & Rahman, A. Strain fluctuations and elastic constants. *J. Chem. Phys.* **76**, 2662 (1982).
39. Wen, B. *et al*. Instabilities in cubic diamond under non-hydrostatic compressive stress. *Diamond and Related Materials* **17**(7–10), 1353 (2008).
40. Libotte, H. & Gaspard, J. P. Pressure induced distortion of the β-Sn phase in silicon: Effect of nonhydrostaticity. *Phys. Rev. B* **62**, 7110 (2000).
41. Gaal-Nagy, K. & Strauch, D. Transition pressures and enthalpy barriers for the cubic diamond –β-tin transition in Si and Ge under nonhydrostatic conditions. *Phys. Rev. B* **73**, 134101 (2006).
42. Cheng, C. Uniaxial phase transition in Si: Ab initio calculations. *Phys. Rev. B* **67**, 134109 (2003).
43. Durandurdu, M. Structural phase transition of gold under uniaxial, tensile, and triaxial stresses: An ab initio study. *Phys. Rev. B.* **76**, 024102 (2007).
44. Korotaev, P., Pokatashkin, P. & Yanilkin, A. The role of non-hydrostatic stresses in phase transitions in boron carbide. *Comput. Mater. Scie.* **121**, 106 (2016).
45. Kulkarni, A. J. *et al*. Novel Phase Transformation in ZnO Nanowires under Tensile Loading. *Phys. Rev. Lett.* **97**, 105502 (2006).
46. Chang, K. J & Cohen, M. L. Ab initio pseudopotential study of structural and high-pressure properties of SiC. *Phys. Rev. B* **35**(15), 8196 (1987).
47. Churcher, N., Kunc, K. & Heine, V. Ground state properties of the group IV ionic compound silicon carbide. *Solid State Commun.* **56**, 177 (1985).
48. Dentenner, P. J. H. & van Haeringen, W. Ground-state properties of polytypes of silicon carbide. *Phys. Rev. B* **33**, 2831 (1986).
49. Cohen, M. L. Calculation of bulk moduli of diamond and zinc-blende solids. *Phys. Rev. B* **32**, 7988 (1985).

50. Yean, D. H. & Riter, J. R. Jr. Estimates of isothermal bulk moduli for group iva crystals with the zincblende structure. *J. Phys. Chem. Solids* **32**, 653 (1971).
51. Yoshida, M. *et al*. Pressure-induced phase transition in SiC. *Phys. Rev. B* **48**(14), 10587 (1993).
52. Yoo, W. S. & Matsunami, H. Solid-state phase transformation in cubic silicon carbide. *J. Appl. Phys.* **30**, 545 (1991).
53. Olego, D., Cardona, M. & Vogl, P. Pressure dependence of the optical phonons and transverse effective chareg in 3C-SiC. *Phys. Rev. B* **25**(6), 3878 (1982).
54. Alekasandrov, I. V. *et al*. Equation of state and Raman scattering in cubic BN and SiC at high pressure. *JETP Lett.* **50**(3), 127 (1989).
55. Debernardi, C. *et al*. Raman line widths of optical phonons in 3C-SiC under pressure: First-principles calculations and experimental results. *Phys. Rev. B* **59**(10), 6774 (1999).
56. Karch, K. *et al*. Ab initio calculation of structural and lattice-dynamical properties of silicon carbide. *Phys. Rev. B* **50**(23), 17054 (1994).
57. Cardona, M. Pressure dependence of dynamical charges and iconicity of semiconductions. *J. Phys. (Paris), Colloq.* **45**, C8–29 (1984).
58. Refson, K., Tulip, P. R. & Clark, S. J. Variational density-functional perturbation theory for dielectrics and lattice dynamics. *Phys. Rev. B* **73**, 155114 (2006).
59. Hohenberg, P. & Kohn, W. Inhomogeneous electron gas. *Phys. Rev. B* **136**, 864 (1964).
60. Kohn, W. & Sham, L. J. Self-consistent equations including exchange and correlation effects. *Phys. Rev. A* **140**, 1133 (1965).
61. Clark, S. J. *et al*. First principlemethods using CASTEP. *Zeitschrift für Kristallographie* **220**, 567 (2005).
62. Perdew, J. P., Burke, K. & Ernzerhof, M. Generalized gradient approximation made simple. *Phys. Rev. Lett.* **77**, 3865 (1996).
63. Hamann, D. R., Schluter, M. & Chiang, C. Norm-conserving pseudopotentials. *Phys. Rev. Lett.* **43**, 1494 (1979).
64. Nielsen, O. H. & Martin, R. M. First-principles calculation of stress. *Phys. Rev. Lett.* **50**, 697 (1983).
65. Gonze, X. First-principles responses of solids to atomic displacements and homogeneous electric fields: Implementation of a conjugate-gradient algorithm. *Phys. Rev. B* **55**, 10337 (1997).
66. Porezag, D. & Pederson, M. R. Infrared intensities and Raman-scattering activities within density-functional theory. *Phys. Rev. B* **54**, 7830 (1996).
67. Van Camp, P. E., Van Doren, V. E. & Devreese, J. T. Ground-state and electronic properties of covalent solids. *Phys. Rev. B.* **38**, 12675 (1988).
68. Priya, V. *et al*. Interaction potential for silicon carbide: A molecular dynamics study of elastic constants and vibrational density of states for crystalline and amorphous silicon carbide. *J. Appl. Phys.* **101**(10), 103515 (2007).
69. Strossner, K., Cardona, M. & Choyke, W. J. High pressure X-ray investigations on 3C-SiC. *Solid State Commun.* **63**, 113 (1987).
70. Li, Z. & Bradt, R. C. The single-crystal elastic constants of cubic (3C) SiC to 1000 °C. *J. Materials Science* **22**, 2557 (1987).

Acknowledgements

Author Contributions

L.L. designed the calculations, analyzed results and wrote the article; Y.L. analyzed data and discussed results; L.Y. performed the analysis with constructive discussions. L.H. helped design the calculations. Z.C. performed the analysis with constructive discussions and improved the English writing. Y.L. and L.G. helped complete the calculation. All the authors have reviewed and approved the final version of this manuscript.

Additional Information